Vibrational structure and partial rates of resonant Auger decay of the N $1s \rightarrow 2\pi$ core excitations in nitric oxide

E. Kukk,[1,2] J.D. Bozek,[2,†] G. Snell,[1,2] W.-T. Cheng,[3] and N. Berrah[1]

[1]*Department of Physics, Western Michigan University, Kalamazoo, MI 49008-5151*

[2]*Lawrence Berkeley National Laboratory, University of California – Berkeley, CA 94720*

[3]*Department of Physics, National Central University, Chung-Li, Taoyuan, Taiwan, 32054, R.O.C.*

Abstract

High-resolution resonant Auger electron spectra of NO measured in the vicinity of the N $1s \rightarrow 2\pi$ core excitations are presented. The open shell electronic configuration of the molecule results in four excited electronic states, three of which are populated in the photoabsorption spectrum, $^2\Delta$, $^2\Sigma^-$ and $^2\Sigma^+$. Electron emission spectra obtained at different vibrational levels of the three N $1s$ core-excited states of NO are reported. Recently reported *ab initio* calculations [J. Chem. Phys. **106**, 4038 (1997)] are used to generate theoretical spectra for comparison with the experimental results taking lifetime vibration interference and Auger resonant Raman effects into account. Very good agreement is found for the lowest energy $X\ ^1\Sigma^+$ final ionic state. Spectra of the higher energy final ionic states are decomposed into contributions from the different $5\sigma^{-1}2\pi^1$ and $1\pi^{-1}2\pi^1$ configurations for comparison of the calculated and experimental partial Auger decay rates. A revised value for the adiabatic ionization energy of the $^1\Delta$ ionic state results from the deconvolution.

[†]Electronic address: JDBozek@lbl.gov

I. INTRODUCTION

Auger electron spectroscopy of molecules is a valuable tool for investigating the electronic structure and potential energy surfaces of molecules [1, 2]. Auger electron spectra can also provide insight into the electronic transitions underlying core-level photoabsorption resonances, particularly in the case of resonant photoexcitation of small molecules. Electronic and vibrational structure of Auger spectra, and changes that occur with the photoexcitation energy, can reveal considerably more details about the core-excitation process and the nature of the core-excited states than can be obtained from the photoabsorption spectra alone. Molecular Auger spectra typically have a complex structure due to the numerous electronic states and vibrational levels that are involved in the decay process. Detailed experimental studies at high photon and electron energy resolution have become possible only recently with the advent of 3rd generation synchrotron radiation sources[3–8].

Significant efforts have been made towards performing accurate calculations of the electronic structure and potential energy curves of small molecules, mostly concentrating on the ground and ionic states, although a few studies of core-excited states are available [3, 5, 9–12]. An accurate interpretation of a molecular resonant Auger spectrum requires a thorough understanding of the core-excitation process and a characterization of the numerous final ionic states of the decay process. Recently this approach has been successfully employed in modeling high-resolution resonant Auger spectra of carbon monoxide [6], for example. Among the diatomic molecules, nitric oxide offers an interesting case due to its open-shell configuration with several differently coupled core-excited electronic states.

In this work, motivated by recently reported *ab initio* calculations [9], we report high-resolution measurements of resonant Auger decay of the 2π excitations at the nitrogen $1s$ edge of NO. In the theoretical work, the excitation of N and O $1s$ core electrons to the 2π valence orbital and the subsequent Auger decay was investigated [9]. However, no detailed comparisons with experiment could be made, since the vibrational and electronic structure was unresolved in the available experimental spectra [13, 14]. In this work, Auger electron spectra are reported at several photon energies across the N $1s \rightarrow 2\pi$ absorption profile,

probing different $\Lambda\Sigma$-coupled electronic states of the N $1s^{-1}2\pi^2$ core-excited configuration. Vibrationally resolved final states in the experimental electron spectra provide a stringent test of the quality of calculated potential energy curves for the core-excited and lowest ionic states. Calculated partial Auger decay rates to several final ionic states are also compared with our experimental results, testing the theory at the level of individual electronic transitions.

The Auger decay spectra of the N $1s$ core-excited states of NO are strongly influenced by lifetime vibrational interference effects as well as the Auger resonant Raman effect, both resulting in line shape distortions and peak position shifts [15]. The interference effects can, in addition, drastically alter the intensity distribution between the vibrational peaks in the spectra. These effects are included in the modeled spectra and are compared with the experimental findings.

II. EXPERIMENT

The experiment was performed at the Advanced Light Source at Beamline 8.0.1 X-ray radiation generated by a 5 cm period undulator was monochromatized by a spherical grating monochromator (SGM) using a grating with 925 lines/mm groove density. A spectrometer based on a Scienta SES-200 hemispherical energy analyzer was used to measure the electron spectra [16]. The target gas was introduced into a gas cell with differentially pumped openings for the photon beam. The end-station is separated from the UHV of the beamline by several differential pumping stages, permitting the use of sample gas pressures up to 10^{-3} Torr within the gas cell. In order to utilize the high resolution of the analyzer in full, the gas cell is equipped with electrodes to compensate for surface potential gradients [17]. The spectrometer was operated in constant (40 eV) pass energy mode.

III. RESULTS AND DISCUSSION

A Theoretical core excitation and Auger decay spectra

Ab initio calculations of the excitation spectrum of the N $1s \rightarrow 2\pi$ resonance and its Auger decay spectra, using a multiconfiguration coupled electron pair approximation method, have been published recently [9]. The emphasis in these calculations was on obtaining accurate potential energy curves (PECs) of the neutral ground and core-excited states of NO, but the PECs of the final ionic states were calculated using less accurate basis sets. Among the main objectives of that study was a calculation of the electronic transition matrix elements for the core-excitation and Auger decay to various final ionic states, thus providing partial Auger decay rates. Comparison of these calculations with the experimental results available at the time required a convolution of the theoretical results with a 1.7 eV wide Gaussian line shape to simulate the moderate experimental resolution in the experimental spectra [13, 14]. To fairly compare the theory with our present experimental results, we have regenerated theoretical spectra using the parameters from Ref. [9] according to our experimental conditions, as described below.

When the individual vibronic peaks in photoabsorption spectrum overlap strongly, the core excitations to and Auger decay from the discrete vibrational levels cannot be treated separately for each level due to strong vibrational lifetime interference effects [15]. Under such conditions, the intensity of photoexcitation and Auger decay, which must be treated as a one-step process, (through the vibrational levels ν of the intermediate electronic states n) to a particular vibrational level ν' that belongs to electronic final state f, is given by the Kramers-Heisenberg formula under resonant Raman conditions [3, 18–20]

$$I_{f\nu'}(\epsilon_{el}) = \sum_c \left| \sum_{n\nu} \frac{\left\langle f\nu' | M^c_{nf} | n\nu \right\rangle \langle n\nu | D_n | 0 \rangle}{\hbar\omega - (E_{n\nu} - E_0) + \frac{i}{2}\Gamma} \right|^2 P(\hbar\omega). \quad (1)$$

Here $|f\nu'\rangle$, $|n\nu\rangle$, and $|0\rangle$ stand for the vibronic wave functions of the final ionic, core-excited intermediate, and ground state respectively and $E_{f\nu'}$, $E_{n\nu}$, and E_0 are the corresponding energies. The energy of the emitted electron is $\epsilon_{el} = \hbar\omega - E_0 + E_{f\nu'}$ and $P(\hbar\omega = \hbar\omega_m + \epsilon)$ is the monochromator function, which in the present case is well described by a Gaussian

distribution centered at $\hbar\omega_m$ with the experimental FWHM. Γ is the lifetime width of the intermediate state, D_n is the dipole operator of the photoexcitation and M_f^c is the Coulomb operator of the Auger decay to the final electronic state f with the outgoing Auger channel c. Here we assume that the final state is stable against further decay and therefore has negligible natural width. The nonresonant term, populating the same ionic states, is omitted in equation (1), since this channel has much smaller cross-section at the resonance energies.

Equation (1) accounts for vibrational lifetime interference effects within the vibrational progression of a single core-excited electronic state as well as for the interference effects between the excitation and decay of different electronic states. Both appear as cross-terms under the square of the summation over $n\nu$. Equation (1) also accounts for the Auger resonant Raman effect, where the line widths and shapes in the Auger electron spectra are determined by the product of the monochromator function $P(\hbar\omega)$ and a function obtained by the summation over c.

To produce the theoretical Auger spectrum from the parameters given in Ref. [9] we used a somewhat simplified formula,

$$I_{nf\nu'}(\epsilon_{el}) = \langle f|M_{nf}|n\rangle^2 \langle n|D_n|0\rangle^2 \left| \sum_{\nu} \frac{\langle \nu'|\nu\rangle \langle \nu|0\rangle}{\hbar\omega - (E_{n\nu} - E_0) + \frac{i}{2}\Gamma} \right|^2 P(\hbar\omega). \qquad (2)$$

Here, the matrix elements $\langle \nu'|\nu\rangle$ and $\langle \nu|0\rangle$ are the overlap integrals of the nuclear wavefunctions. The vibrational energy levels and nuclear wavefunctions for Morse potentials were obtained by solving the nuclear Shrödinger equations numerically. The vibrational progressions in the Auger spectra were calculated separately for every combination of the core-excited state n and final electronic state f. The progressions were then added to the total theoretical spectrum with the weight factors as products of the calculated oscillator strengths for creating the core-excited state n and its partial decay rate to the final state f.

The set of parameters used to generate the Morse potentials and nuclear wavefunctions is given in Table I. A Gaussian function with a FWHM of 130 meV was used for the monochromator function $P(\hbar\omega)$ according to our experimental conditions. Theoretical values from Ref. [9] were used for the equilibrium bond distances, vibrational spacings and anharmonicities of the ground and core-excited states. The parameters for the PEC of the

lowest ionic state $X\ ^1\Sigma^+$ were also given in Ref. [9], which we used to calculate the vibrational progressions associated with this state in the Auger electron spectra. Since the accuracy of the calculated ionization energies in Ref. [9] is only moderate, particularly for the higher-lying ionic states, we used experimentally determined parameters for the PECs and the binding energies of the ionic states [21] instead of theoretical values. Similarly, the adiabatic ionization energies for the core-excited states given in Table I are experimental values from Ref. [22]. Using accurate energy positions in the Auger electron spectrum is especially important at the higher binding energy region, where the vibrational progressions of several electronic states overlap strongly and energy shifts would make a comparison with the experimental spectrum impossible.

Expression (2) accounts for the LVI within the excitation and decay of a single core-excited electronic state n, but the interference effects between different electronic decay channels are disregarded. The relative phases of the electronic matrix elements of the core-excitation and Auger decay are therefore not needed. This approximation is not severe in most cases, as there is little overlap of transitions originating from different core-excited electronic states to the same final ionic state at any of the excitation energies. The effects of inter-state interference are expected to be the strongest for the $^{1,3}\Pi$ states, which has contributions to the Auger decay from all three core-excited states.

The line shapes in the Auger spectra calculated according to equation (2) are based on the Lorentzian shape with the natural width, narrowed by the monochromator function and distorted by the interference effects. In order to account for the broadening due to the spectrometer function and other factors (Doppler broadening), the calculated spectra were further convoluted by a Gaussian with an 80 meV FWHM.

B Nitrogen $1s$ photoexcitation to the 2π orbital

The first and strongest pre-edge structure in N $1s$ photoabsorption spectrum is due to excitation of the N $1s$ electron to the 2π valence orbital, which is only partially filled in the ground electronic state of NO, $1\sigma^2 2\sigma^2 3\sigma^2 4\sigma^2 1\pi^4 5\sigma^2 2\pi^1 (X\ ^2\Pi)$. In the electronic

configuration of NO, the 1σ and 2σ orbitals correspond closely to the atomic $1s$ orbitals of oxygen and nitrogen, respectively. The atomic notation of these orbitals will be used throughout this study. Four $\Lambda\Lambda$-coupled states – $^2\Sigma^-$, $^2\Sigma^+$, $^2\Delta$ and $^4\Sigma^-$ – are possible for the N $1s^{-1}2\pi^2$ core-excited electronic configuration. Only the three doublet states are observed in the experimental photoabsorption spectrum however [9]. The photoabsorption spectrum of NO in the region of N $1s \rightarrow 2\pi$ excitations is shown in Fig. 1. Due to several strongly populated vibrational levels for each electronic state, the transitions to the three electronic excited states states overlap strongly. It has been possible, however, to decompose the spectrum into the vibrational bands of individual electronic transitions [22].

We used narrow bandpass (about 130 meV FWHM) synchrotron radiation to selectively excite individual vibrational levels of the core-excited electronic states. The photon energies at which Auger decay spectra were measured are indicated by the labels A-G in Fig. 1. Excitation energies and their corresponding vibronic levels are listed in Table II.

Calculated vibrational progressions of the three excited states are also shown in Fig. 1. These curves are reproduced according to Ref. [9], with the relevant parameters listed in Table I. To obtain better agreement with the measured absorption profile, we applied the same corrections used in Ref. [9], namely experimental adiabatic excitation energies were used and the linewidths were increased from calculated widths of 111-115 meV to the experimental value of 130 meV [22].

C Auger decay of the N $1s^{-1}2\pi^2$ configuration

1 General features

Electron emission spectra measured at several photon energies across the N $1s \rightarrow 2\pi$ resonance are shown in the left panel of Fig. 2. Theoretical Auger electron spectra (obtained by methods described in Section III.A and using the parameters of Table I) are shown in the right panel of Fig. 2. A value of 130 meV was used for the natural widths of the core- excited states when calculating the Auger electron spectra. Both the theoretical and experimental spectra are normalized to equal maximum peak intensity for ease of comparison and do not

represent the decrease of cross-section away from the resonance maximum. The binding energy range of the the electron spectra in the figure covers final ionic states with single vacancies in the 2π, 5σ and 1π orbitals, states that can be created both by direct valence photoionization and by resonant Auger decay of the core-excited state. The uppermost spectrum (V) in Fig. 2 was measured at a photon energy of 380 eV, well below the resonance structure in the absorption spectrum, and is due only to direct valence ionization. Spectrum (V) was measured with lower photon and electron energy resolution to compensate for the much smaller cross section of the direct valence photoionization at these high photon energies The cross-section for nonresonant valence photoionization is, according to these measurements, at least an order of magnitude less than that of any of the resonant spectra shown in the figure. Significant changes in the relative intensities of the electronic bands and their vibrational progressions can be seen at the resonant photon energies (A-G). The dominant bands in the nonresonant spectrum (V) are associated with the $X\ ^1\Sigma^+$ and $^{1,3}\Pi$ ionic states, whereas in the resonant spectra the Auger decay leads to a larger number of ionic states with $2\pi^0$, $5\sigma^{-1}2\pi^1$ and $1\pi^{-1}2\pi^1$ configurations as given in Table I.

The assignment and adiabatic ionization energies of the structures observed in the electron spectra are given in Table I. The low-binding-energy part of the spectrum displays the well separated $X\ ^1\Sigma^+$ band, whereas the region above 16 eV shows a complex structure due to the transitions to a number of final states. The different character of these two regions in the spectra warrants a separate analysis, since for the $X\ ^1\Sigma^+$ state a more accurate comparison of the experimental and theoretical vibrational progressions can be made.

The set of spectra shown in Fig. 2 represents the excitation - de-excitation of the ν=0 and 1 vibrational levels of the three core-excited states. The relative decrease in the intensity of the $X\ ^1\Sigma^+$ band in the spectra (C) and (E) is due to the fact that these spectra originate mostly from the $^2\Sigma^-$ core-excited state, which does not decay into the $X\ ^1\Sigma^+$ state.

In earlier measurements of the N $1s^{-1}2\pi^2$ Auger decay spectra [14], selective population of the $^2\Delta$, $^2\Sigma^-$ and $^2\Sigma^+$ core-excited states was achieved, although not of their individual vibrational levels. Clear changes in the structure in the 16-19 eV binding energy region of the Auger electron spectra were observed, depending on the core-excited state populated. It

was concluded, that the $^2\Delta$ and $^2\Sigma^+$ states decay primarily to the singlet and the $^2\Sigma^-$ state to the triplet ionic states, a finding that is in general agreement with the present results.

2 Auger decay to the $X\ ^1\Sigma^+$ ionic state

The region of the $X\ ^1\Sigma^+$ final ionic state in the Auger electron spectra is expanded in Fig. 3 showing the decay of the ν=0, 1 and 2 levels of the $^2\Delta$ core-excited state (A, B, D) and the ν=0 and 1 levels of the $^2\Sigma^+$ state (F, G).

There is excellent overall agreement between the experiment [left] and calculation [right] for the decay of the ν=0, 1 and 2 vibrational levels [spectra (A),(B) and (D), respectively] of the $^2\Delta$ state. Spectrum (C) represents Auger decay under detuned conditions, since the photon energy of the excitation falls in between the ν=1 and 2 peaks of the $^2\Delta$ state (no contributions to this final state are predicted from the $^2\Sigma^-$ state). Spectra (F) and (G) are assigned to the decay of the ν=0 and 1 levels of the $^2\Sigma^+$ state, but, as can be seen from Fig. 1, have some contribution from the decay of higher vibrational levels of the $^2\Delta$ state. This contribution is readily visible in Fig. 3 as population of high vibrational levels of the final state – $\nu' \geq 9$ in spectrum (F) and $\nu' \geq 11$ in spectrum (G) – since transitions from the $^2\Sigma^+$ state to these levels have negligible intensity. Minor discrepancies can be observed between the experiment and theory in spectra (F) and (G). These can be due to small errors in the calculated shapes of the PECs, but can also be caused by the interference between the Auger decay of the $^2\Sigma^+$ and $^2\Delta$ state, which is not included in the modeled spectra. Note that for the $X\ ^1\Sigma^+$ final state, the theoretical PEC parameters [9](Table I) that were used are very close to the experimentally determined ones (r_e=1.063 Å, ω_e=295 meV, $\omega_e x_e$=2.0 meV [21]), and therefore any minor discrepancies between the experimental and theoretical spectra are probably due to errors in the calculation of the core-excited states. Experimental ionization energies were used for the core-excited and the $X\ ^1\Sigma^+$ state.

The line shapes in the Auger electron spectra of Fig. 3 are not well represented by either Gaussian or Voigtian profiles. The distortions to the peak shapes are most apparent for the low intensity peaks, such as ν'=0, 5 and 6 in spectrum (C). One reason for the lineshape

distortions is the Auger resonant Raman effect. In the present case, the photon bandwidth was approximately equal to the natural width of 130 meV. Under such conditions, the line shape is not represented by a simple analytical curve [15]. Furthermore, if the maximum of the photon energy band is detuned from the peak maximum of the resonance (as for spectrum (C)), the Auger resonant Raman effect results in asymmetric line shapes and shifts the peak maxima. These effects are taken into account in equations (1) and (2).

The Auger electron spectra of Fig. 3 are strongly influenced by LVI. The effect is highlighted in Fig. 4, showing the Auger decay of the $\nu = 1$ level of the $^2\Delta$ state (photon energy position B in Fig. 1). The calculated spectrum is decomposed into direct and interference components, the latter being defined as cross-terms under the square in equation (2). The LVI affects peak intensities as well as their shapes and positions. The peak shifts and distorted shapes can be observed also in the experimental spectrum. (The systematic shift of the positions of the calculated peaks towards higher binding energies, which is more prominent for higher ν', is caused by the calculated vibrational constant being 4 meV larger than its experimental value.) It is interesting to note a change in the interference contributions for $\nu' > 5$, which are destructive rather than constructive in the case of the lower vibrational levels. This behavior is typical for all spectra in Fig. 3. It is due to the fact that the Franck-Condon integrals of the Auger decay from neighboring levels of the core-excited state tend to have the same sign for the lower levels of the final ionic state, but alternate signs for higher levels. This kind of interference pattern was calculated also by Carroll *et al.* [23], but a direct comparison of individual vibrational peaks with experiment could not be made at the time.

The extent of the LVI effects on the overall shape of the electronic band depends on the breadth of the photon band. Using broad excitation bandwidth results in many vibrational levels of the core-excited state being excited simultaneously and the LVI effects become more pronounced, as can be seen from Ref [9], where a bandwidth of 700 meV was used in the simulation.

Auger decay spectra from the lowest vibrational levels of the $^2\Delta$, $^2\Sigma^-$ and $^2\Sigma^+$ states are shown in detail in Figs. 5, 6 and 7, respectively. The binding energy region of Figs. 5-7 corresponds to ionic states with $5\sigma^{-1}2\pi^1$ and $1\pi^{-1}2\pi^1$ configurations. The experimental spectra are compared with calculated curves, for which the contributions to the total intensity from each final ionic state are shown. The experimental and calculated curves were normalized to equal total intensity, including the $X\ ^1\Sigma^+$ band. The parameters used for the calculations were the same as those used for Fig. 2.

The Auger decay spectrum of the $^2\Delta(\nu = 0)$ state (Fig. 5) was measured at the photon energy position A of Fig. 1. According to the calculations, there is significant Auger decay rate only to four final states in the binding energy range shown. The enhanced background between 16.7 and 17.2 eV is due to the decay of the $^2\Sigma^-$ state, which is also weakly excited at this photon energy. For this process, partial contributions are not shown.

The use of experimental binding energies for the final states [21] results in a good alignment of the calculated curves with the peaks in the experimental spectrum. The exception is the $^1\Delta$ ionic state, for which the binding energy of 18.07 is given with large uncertainty in Ref. [21] due to problems in assigning the vibrational peaks in the photoelectron spectrum. Using this energy resulted in obvious misalignment of the calculated vibrational profile with respect to the measured spectra. A new binding energy of 18.19 eV was determined for this state through a least squares fit of the calculated profiles to the experimental data. This value was used in the calculated spectra at all photon energies.

General agreement between the calculation and experiment is good in Fig. 5. The relative intensity of the $^1\Pi$ band in the calculated spectrum is somewhat smaller than in the experiment. This discrepancy could be partly due to the contributions from and interference with the direct valence photoionization, where the transitions to this final ionic state have a relatively large cross-section.

In order to obtain an experimental estimate of the partial Auger decay rates, the calculated vibrational profiles were fit to the measured spectrum, treating the partial Auger

rates as free parameters. The results are given in Table III, where both the theoretical and experimental values are scaled to give a total rate of unity over the states listed. The bands for which the calculated intensity is very small were not included in the fit.

The experimental and calculated Auger decay spectra of the $^2\Sigma^-(\nu = 0)$ core-excited state shown in Fig. 6, measured at the photon energy position C of Fig. 1, agree fairly well. The final states populated from this core-excited state are different than those from the $^2\Delta(\nu = 0)$ state (Fig. 5), except for the $^{1,3}\Pi$ states that are present in both spectra. Contributions from the decay of the higher vibrational levels of the $^2\Delta$ state build up the spectrum above 18.1 eV binding energy. Discrepancies between the experiment and calculation are stronger in this region of the spectrum, probably because the calculated vibrational profiles are more sensitive to errors in Morse potentials when originating from higher levels of the core-excited states. The calculated profiles were also fit to the experimental data in this range to evaluate the Auger transition rates, and the results are summarized in Table III. Note that the intensity of the $^3\Pi$ peak has large uncertainty due to overlap with the strong background structure.

Auger decay spectrum of the $^2\Sigma^+$ core-excited state are shown in Fig. 7, measured at the photon energy F of Fig. 1. At this energy, there is a strong overlap between the vibrational levels of all three core-excited states in the absorption spectrum. Consequently, a large fraction of the intensity in Fig. 7 is due to the decay of the higher vibrational levels of the $^2\Delta$ and $^2\Sigma^-$ states. Contributions from the $^2\Sigma^+$ state are present mostly above 18.0 eV binding energy, showing a fair agreement between theory and experiment. Results of a least-squares fit of the individual profiles to the data is given in Table III. The intensity of the $^3\Pi$ band cannot be determined accurately because of strong overlap with other final states. The agreement of the contributions from other core-excited state is worse, again probably because higher vibrational levels of the excited and final ionic states are involved.

IV. CONCLUSIONS

Vibrationally resolved resonant Auger electron spectra from the decay of the $^2\Delta$, $^2\Sigma^-$ and $^2\Sigma^+$ core-excited states of the N $1s^{-1}2\pi^2$ configuration of NO were compared with the results of *ab initio* calculations. Very good agreement was found between the experimental and theoretical vibrational progressions of the $X\ ^1\Sigma^+$ band, indicating that the calculated potential energy curves describe the ground, core-excited and final ionic electronic states involved in the transition very well. In the higher binding energy region, the spectra were decomposed into partial contributions from the decay to different final ionic states. Here, the primary objective was to compare the calculated partial Auger decay rates with the experiment. A good agreement was found in the decay from the lowest levels of the core-excited states for all final states with $2\pi^0$, $5\sigma^{-1}2\pi^1$ and $1\pi^{-1}2\pi^1$ configurations. The largest discrepancies (up to 1.5 times) were found in the case of the $^{1,3}\Pi$ ionic states, which could be partially attributed to the contributions from direct ionization, interference effects and inaccuracies of the fitting procedure. In addition, a new value of the adiabatic ionization energy of the $^1\Delta$ ionic state was obtained from least-squares analysis of the spectra.

ACKNOWLEDGMENTS

This work was supported by the Department of Energy, Office of Science, Basic Energy Sciences, Chemical Sciences Division. The Advanced Light Source and JDB are supported by the Director, Office of Science , Office of Basic Energy Sciences, of the U.S. Department of Energy under Contract No. DE-AC03-76SF00098. We are thankful to S.E. Canton-Rogan for help with the experiment.

REFERENCES

[1] W. Eberhardt, J.-E. Rubensson, K.J. Randall, J. Feldhaus, A.L.D. Kilcoyne, A.M. Bradshaw, Z. Xu, P.D. Johnson, and Y. Ma, Physica Scripta **T41**, 143 (1992).

[2] H. Aksela and S. Aksela, J. Electron. Spectrosc. Relat. Phenom. **100**, 395 (1999).

[3] M.N. Piancastelli, M. Neeb, A. Kivimäki, B. Kempgens, H.M. Köppe, K. Maier, A.M. Bradshaw and R.F. Fink, J. Phys. B **30**, 5677 (1997).

[4] S.J. Osborne, S. Sundin, A. Ausmees, S.L. Sorensen, A. Kikas, and S. Svensson, J. Electron. Spectrosc. Relat. Phenom. **95**, 25 (1998).

[5] R. Püttner, I. Dominguez, T.J. Morgan, C. Cisneros, R.F. Fink, E. Rotenberg, T. Warwick, M. Domke, G. Kaindl, and A.S. Schlachter, Phys. Rev. A **59**, 3415 (1999).

[6] E. Kukk, J.D. Bozek, W.-T. Cheng, R.F. Fink, A.A. Wills, and N. Berrah, J. Chem. Phys. **111**, 9642 (1999).

[7] M.N. Piancastelli, B.Kempgens, U. Hergenhahn, A. Kivimäki, K. Maier, A. Rüdel, and A.M. Bradshaw, Phys. Rev. A **59**, 1336 (1999).

[8] E. Kukk, J.D. Bozek, and N. Berrah, Phys. Rev. A, in print.

[9] R. Fink, J. Chem Phys. **106**, 4038 (1997).

[10] Z.W. Gortel, R. Teshima, and D. Menzel, Phys. Rev. A **58**, 1225 (1998).

[11] R.F. Fink, M. Kivilompolo, and H. Aksela, J. Chem. Phys. **111**, 10034 (1999).

[12] R.F. Fink, S.L. Sorensen, A. Naves de Brito, A. Ausmees, and S. Svensson, J. Chem. Phys. **112**, 6666 (2000).

[13] T.X. Carroll and T.D. Thomas, J. Chem. Phys. **97**, 894 (1992).

[14] T.X. Carroll, M. Coville, P. Morin, T.D. Thomas, J. Chem. Phys. **101**, 998 (1994).

[15] E. Kukk, S. Aksela, and H. Aksela, Phys. Rev. A, **53**, 3271 (1996).

[16] N. Berrah, B. Langer, A.A. Wills, E. Kukk, J.D. Bozek, A. Farhat and T.W. Gorczyca J. Electron Spectrosc. Relat. Phenom. **101**, 1 (1999).

[17] P. Baltzer, L. Karlsson, M. Lundqvist and B. Wannberg, Rev. Sci. Instrum. **64**, 2179 (1993).

[18] M. Neeb, J. E. Rubensson, M. Biermann, W. Eberhardt, J. Electron Spectrosc. Relat. Phenom. **67,** 261 (1994).

[19] T. Åberg and G. Howat, in *Handbuch der Physik*, edited by W. Melhorn (Springer-Verlag, Berlin, 1982), Vol. NUI, p. 469; T. Åberg, Physica Scripta **T41**, 71 (1992).

[20] A. Kivimäki, A. Naves de Brito, A. Aksela, H. Aksela, O.-P. Sairanen, A. Ausmees, S.J. Osborne, L.B. Dantas, and S. Svensson, Phys. Rev. Lett. **71**, 4307 (1993).

[21] D.L. Albritton, A.L. Schmeltekopf, and R.N. Zare, J. Chem. Phys. **71**, 3271 (1979).

[22] G.Remmers, M. Domke, A. Puschmann, T. Mandel, and G. Kaindl, Chem. Phys. Lett. **214**, 241 (1993).

[23] T.X. Carroll, S.E. Anderson, L. Ungier, and T.D. Thomas, Phys. Rev. Lett. **58**, 867 (1987).

FIGURES

FIG. 1: Photoabsorption spectrum of NO covering the region of the N $1s \rightarrow 2\pi$ excitations. Experimental data (circles) is digitized from Ref. [22] and the calculated curves are according to Ref. [9]. The sum of the calculated curves is convoluted by a 75 meV FWHM Gaussian. Labels A-G mark the photon energies at which the resonant Auger electron spectra were measured.

FIG. 2: Experimental (a) and calculated (b) Auger electron spectra of the decay of the N $1s^{-1}2\pi^2$ core-excited states. Labels refer to the excitation energies indicated on Fig. 1.

FIG. 3: Binding energy region of the $X\ ^1\Sigma^+$ final state of the Auger electron spectra. (a) Experiment, (b) calculation. Labels refer to the photon energies indicated on Fig. 1.

FIG. 4: $X\ ^1\Sigma^+$ band in the Auger decay spectrum of the $\nu = 1$ level of the $^2\Delta$ core-excited state. Experiment is compared with calculation, showing direct and interference contributions.

FIG. 5: Auger electron spectrum of the decay of the $^2\Delta$ ($\nu = 0$) core-excited state. Calculated spectrum and vibrational profiles for each final state are shown as line spectra.

FIG. 6: Auger electron spectrum of the decay of the $^2\Sigma^-$ ($\nu = 0$) core-excited state.

FIG. 7: Auger electron spectrum of the decay of the $^2\Sigma^+$ ($\nu = 0$) core-excited state.

TABLES

TABLE I: Adiabatic ionization energy, equilibrium bond distance, vibrational spacing and anharmonicity values used to generate the potential energy curves of the ground, core-excited and ionic states. Oscillator strengths, f, relative to the excitation of the $^2\Sigma^+$ state are also given. The data is from Refs. [9, 21, 22] (see text for details).

	Term	Config.	E(eV)	r_e(Å)	ω_e(meV)	$\omega_e x_e$(meV)	f
NO	$^2\Pi$	$...1\pi^4 5\sigma^2 2\pi^1$	0	1.146	241	1.7	
N*O	$^2\Delta$	N $1s^{-1}2\pi^2$	399.38	1.211	202	2.2	1.95
	$^2\Sigma^-$	N $1s^{-1}2\pi^2$	399.67	1.204	210	2.3	2.43
	$^2\Sigma^+$	N $1s^{-1}2\pi^2$	400.00	1.225	188	2.7	1.00
NO^+	$^1\Sigma^+$	$2\pi^0$	9.26	1.062	298	2.0	
	$^3\Pi$	$5\sigma^{-1}2\pi^1$	16.56	1.176	212	1.8	
	$^3\Delta$	$1\pi^{-1}2\pi^1$	16.87	1.279	163	1.3	
	$^3\Sigma^-$	$1\pi^{-1}2\pi^1$	17.60	1.276	159	1.3	
	$^1\Sigma^-$	$1\pi^{-1}2\pi^1$	17.76	1.287	159	1.6	
	$^1\Delta$	$1\pi^{-1}2\pi^1$	18.19[a]	1.301	151	1.4	
	$^1\Pi$	$5\sigma^{-1}2\pi^1$	18.32	1.194	199	2.5	

[a] This experiment.

TABLE II: Assignment of the N $1s \rightarrow 2\pi$ excitations at the labeled photon energies of Fig. 1.

Label	$h\nu$(eV)	Assignment
A	399.38	$^2\Delta(\nu = 0)$
B	399.56	$^2\Delta(\nu = 1)$
C	399.67	$^2\Sigma^-(\nu = 0)$
D	399.75	$^2\Delta(\nu = 2)$

E	399.95	$^2\Sigma^-(\nu=1)$
F	400.02	$^2\Sigma^+(\nu=0)$,$^2\Sigma^+(\nu=2)$
G	400.17	$^2\Sigma^+(\nu=1)$,$^2\Sigma^+(\nu=3)$

TABLE III: Calculated [9] and experimental partial Auger decay rates from the three terms of the N $1s^{-1}2\pi^2$ core-excited state. The adiabatic ionization energies are from Ref. [21].

			$^2\Delta$		$^2\Sigma^-$		$^2\Sigma^+$	
E(eV)	Term	Configuration	Calc.	Exp.	Calc.	Exp.	Calc.	Exp.
9.26	$^1\Sigma^+$	$2\pi^0$	0.307	0.27	0.000		0.226	0.23
16.56	$^3\Pi$	$5\sigma^{-1}2\pi^1$	0.030	0.03	0.108	0.15	0.032	0.1
16.87	$^3\Delta$	$1\pi^{-1}2\pi^1$	0.001		0.614	0.57	0.004	
17.60	$^3\Sigma^-$	$1\pi^{-1}2\pi^1$	0.001		0.249	0.25	0.000	
17.76	$^1\Sigma^-$	$1\pi^{-1}2\pi^1$	0.270	0.23	0.001		0.000	
18.19[a]	$^1\Delta$	$1\pi^{-1}2\pi^1$	0.218	0.21	0.003		0.540	0.54
18.32	$^1\Pi$	$5\sigma^{-1}2\pi^1$	0.174	0.25	0.025	0.03	0.198	0.13

[a]This experiment.

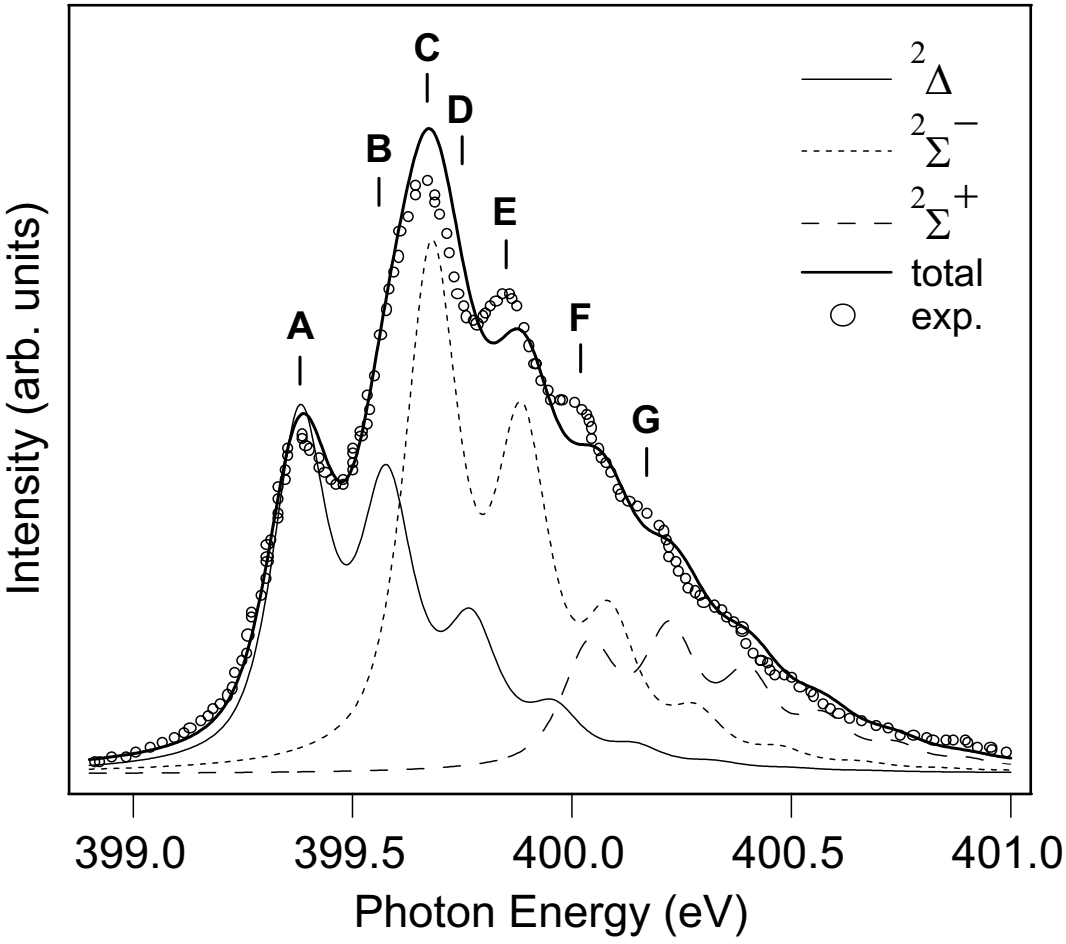

Figure 1 - Kukk *et al.*, Vibrational structure and partial rates...

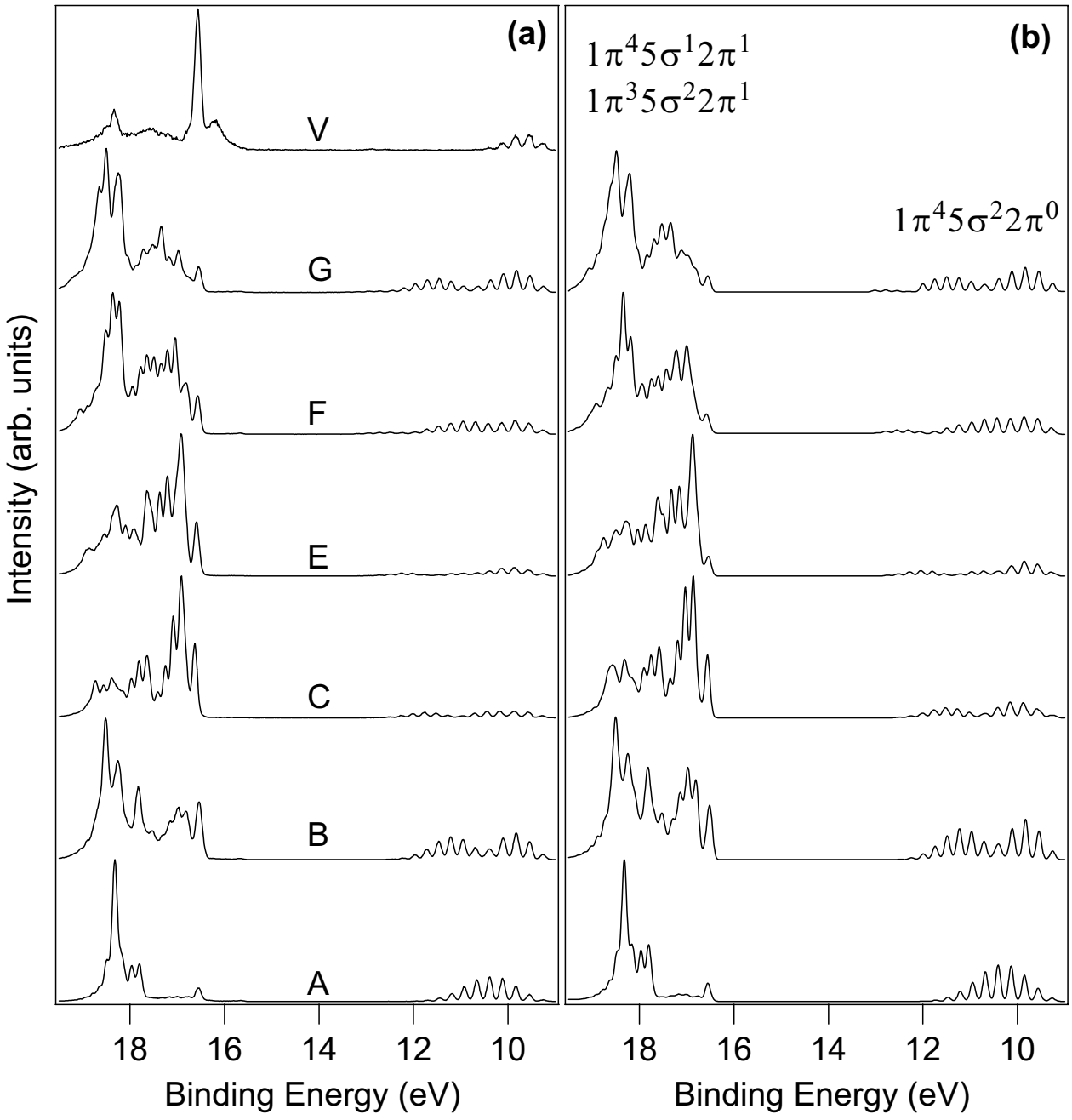

Figure 2 - Kukk *et al.*, Vibrational structure and partial rates...

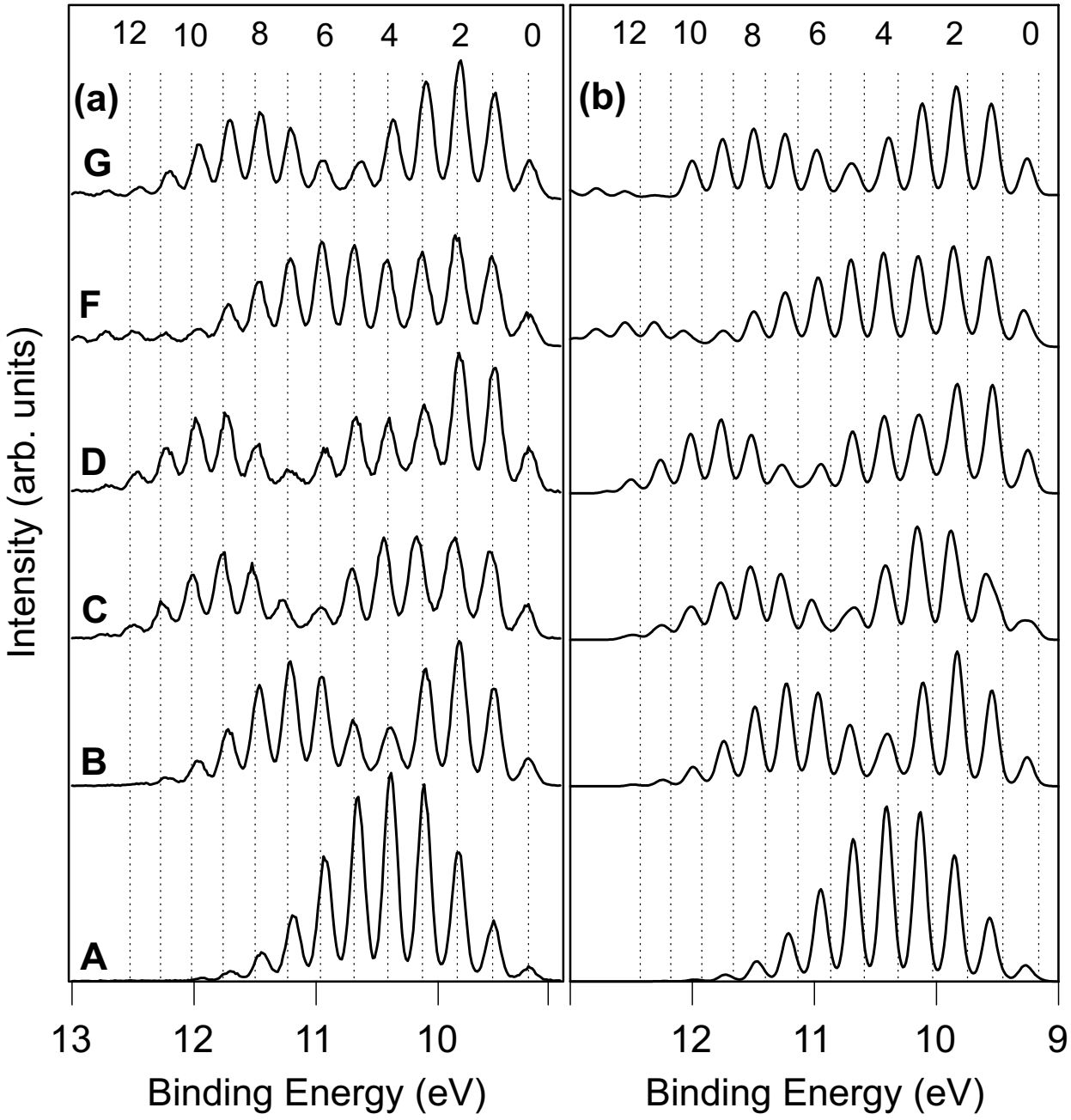

Figure 3 - Kukk *et al.*, Vibrational structure and partial rates...

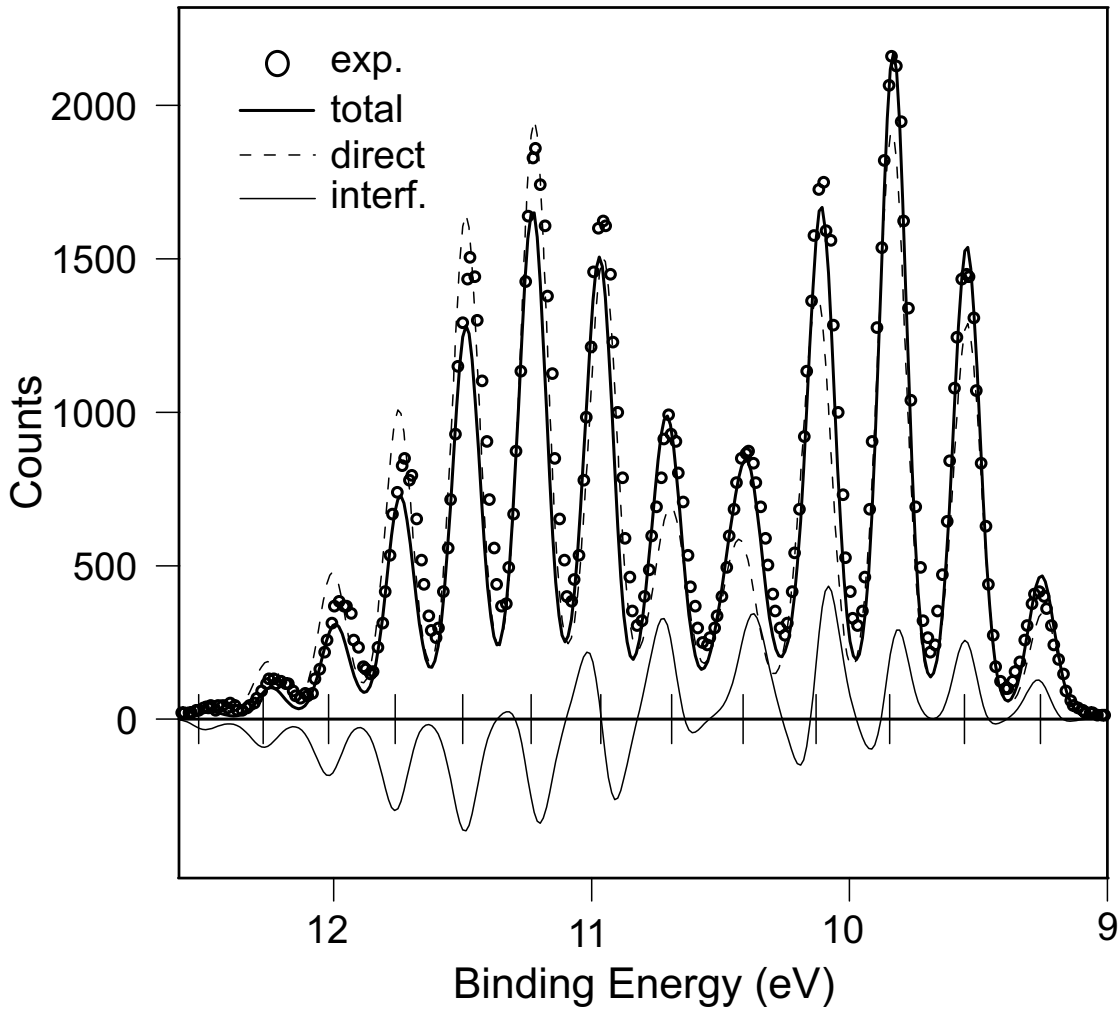

Figure 4 - Kukk *et al.*, Vibrational structure and partial rates...

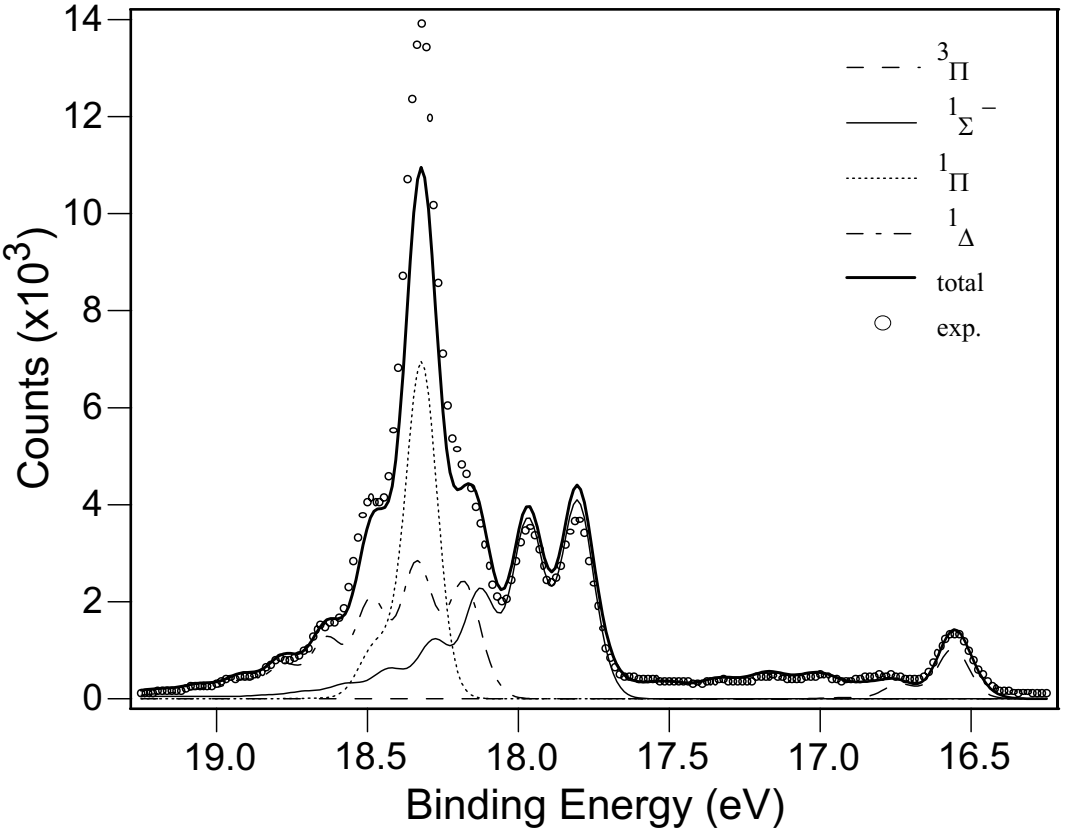

Figure 5 - Kukk *et al.*, Vibrational structure and partial rates...

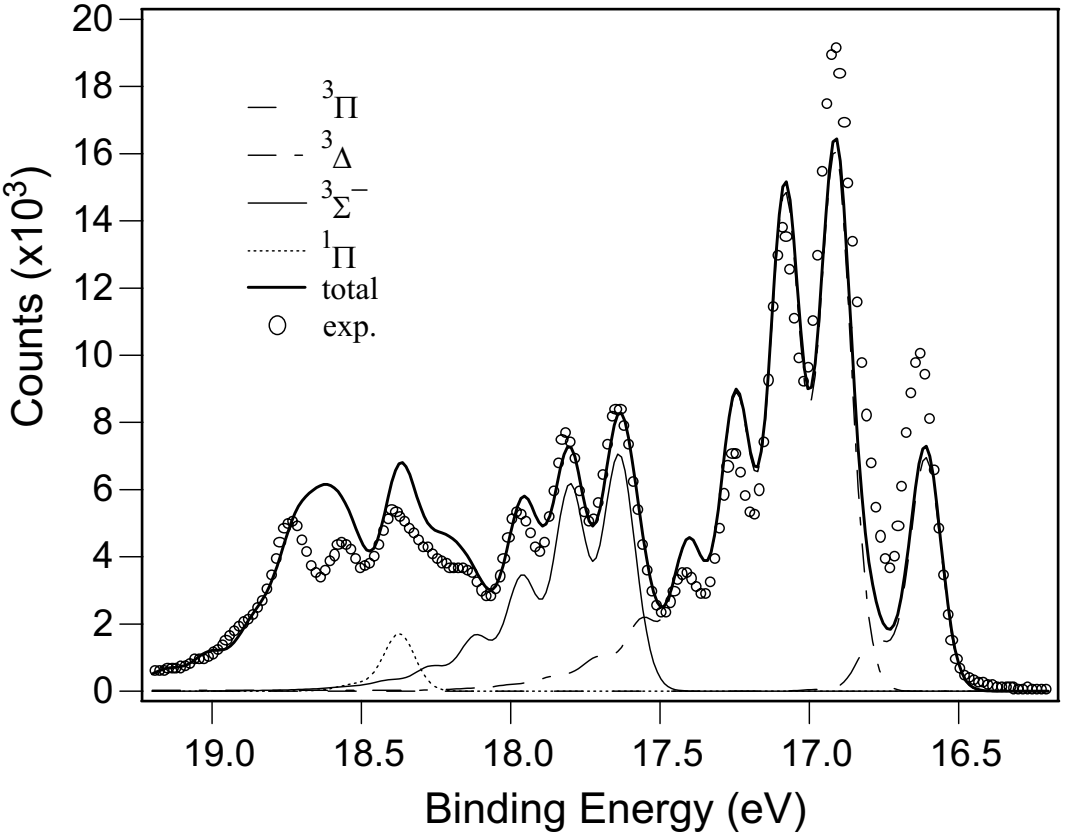

Figure 6 - Kukk *et al.*, Vibrational structure and partial rates...

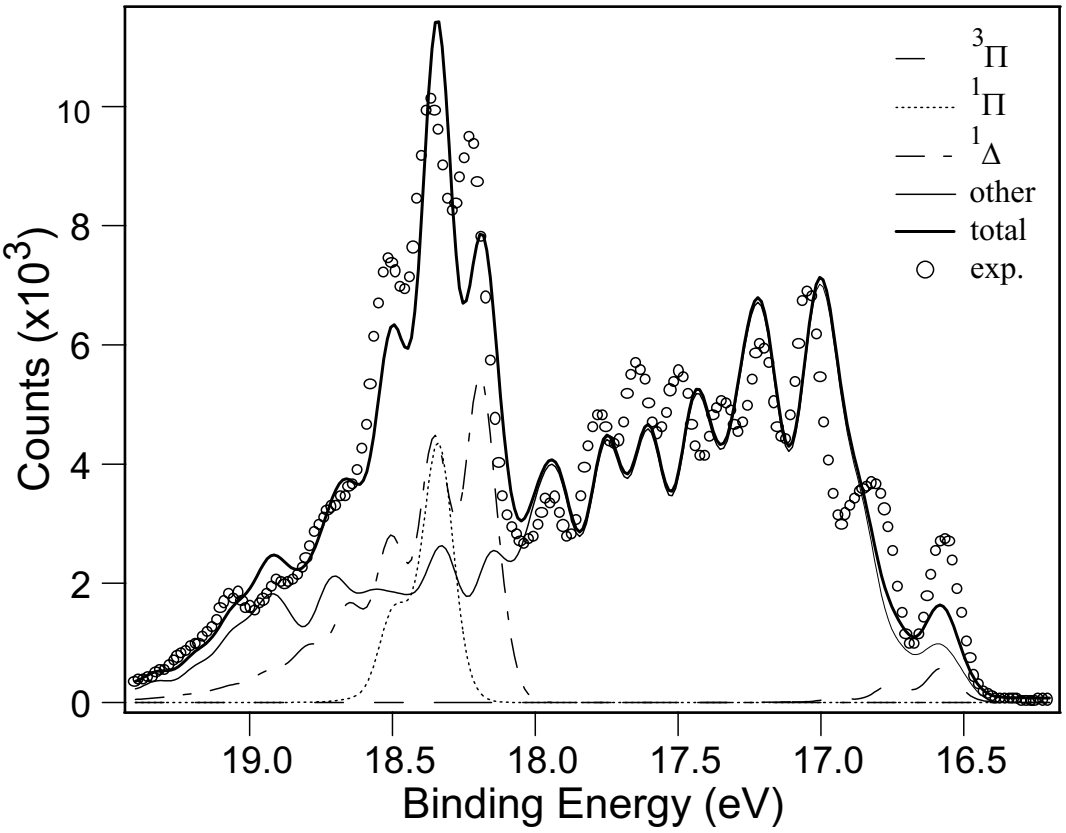

Figure 7 - Kukk *et al.*, Vibrational structure and partial rates...